Rev. Adv. Mater. Sci. 31 (2012) 54-61

THE FORMATION OF ULTRAFINE GRAINED STRUCTURE IN AN Al-Mg-Sc ALLOY BY EQUAL CHANNEL ANGULAR PRESSING AT 150 °C

A. A. Mogucheva, A. V. Dubyna and R. O. Kaibyshev

Belgorod State University, Pobedy 85, Belgorod 308015, Russia

Received: April 20, 2012

Abstract. Effect of equal-channel angular pressing (ECAP) on deformation behavior of an Al–6%Mg–0.5%Mn–0.2%Sc–0.07%Zr (in weight %) alloy denoted as 1570 was considered. The structural changes during deformation were characterized by the elongation of initial grains towards the axis of ECAP and the development of new fine grains. The fraction of fine grains increased with increasing the strain. The ECAP resulted in significant strengthening. The yield strength approached 480 MPa in the specimen processed to ~8, whereas that in the initial state is 250 MPa. The relationship between the deformation microstructure and the tensile behavior is discussed.

1. INTRODUCTION

It has been shown that a significant increase in the strength of aluminum-based alloys can be attained through the formation of an ultrafine grained (UFG) structure by using equal-channel angular pressing (ECAP) [1-6]. Aluminum alloys containing 1.5 to 3 wt.% of Mg produced by ECAP up to an effective strain of ~8 at temperatures of about 200 °C demonstrated yield stresses (YS) of ~400 MPa and ultimate tensile strengths (UTS) of ~420 MPa [3-6]. ECAP resulted in the formation of deformation structure consisting mainly of elongated (sub)grains entirely delimited by low-angle boundaries; very high dislocation density was observed in the subgrain interiors [3,7]. This suggests that the high strengths of none-age hardenable aluminum alloys are attributed to strain hardening. Despite this fact, authors [1] assumed that increased strength of aluminum alloys subjected to ECAP is caused by extensive grain refinement. An efficiency of both the strain hardening and the grain refinement is more pronounced at lower temperatures. Therefore, further increase in the strength can be obtained by decrease of processing temperature, although ECAP at 150 °C to ~5-6 led to failure of the samples as a result of thedevelopment of macroscopic cracks [8].

The mechanical properties of ultrafine grained materials have been investigated in tensile testing by various groups [9-11]. In terms of the effect of grain size on the yield stress both Valiev *et al.* [9] and Furukawa *et al.* [10] concluded that their observations confirmed the Hall-Petch relationship:

$$\sigma = \sigma_0 + kd^{-1/2}, \quad (1)$$

where k and σ_0 are a constant for the material, d is a grain size.

The aim of the present work is to evaluate the effect of ECAP with back pressure at 150 °C with different strains on structure and mechanical properties of an Al-Mg-Sc alloy, and to study the relationship between the deformation microstructures and the tensile behavior.

Corresponding author: A. A. Mogucheva, e-mail: mogucheva@bsu.edu.ru

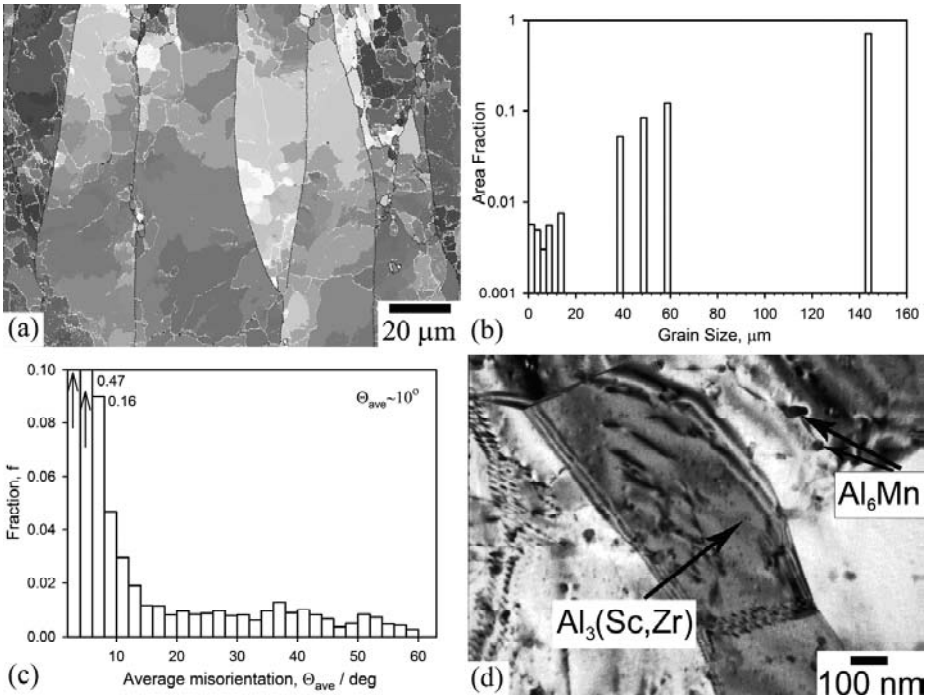

Fig. 1. Typical microstructure of 1570 alloy.

2. EXPERIMENTAL MATERIAL AND PROCEDURES

The experiments were conducted by using an aluminum alloy with a chemical composition of Al-6%Mg-0.5%Mn-0.2%Sc-0.07%Zr (wt.%). This alloy was developed in Russia and designated as 1570. Initially the 1570Al was homogenized at 360 °C for 8 hours and extruded. Billets with a square cross-section of 20×20×100 mm^3 were deformed by ECAP with a back pressure at 150 °C. An isothermal die with a rectangular cross-section of 400 mm^2 and a channel angle Φ of 90° had a horizontal L-shaped configuration [1]. The angle Ψ, which represents the outer arc of the curvature where the two parts of the channel intersect, was equal to ~1°. Deformation through this die produced an imposed strain of ~1 in each passage [1]. The samples strained up to ε~1, 2, 4, and 8 were rotated by 90° around the Z axis between each pass in the same direction, i.e. the route B_c [1] was used. The pressing speed was approximately 3 mm/s.

The methods of optical metallography (OM), transmission electron microscopy (TEM), electron backscattering diffraction (EBSD) analysis were described in previous papers in details [12-14]. Terms 'grain' and 'subgrains' are used for definition of crystallites, which are entirely delimited by high-angle boundaries (HABs) and low-angle boundaries (LABs), respectively [15]. The (sub)grains are crystallites which are bounded partly by LABs and partly by HABs [15]. The misorientations of (sub)grain boundaries were determined using a FEI Quanta 600 SEM fitted with an automated EBSD pattern collection system. Notably, dark and light lines on the EBSD maps indicate the HABs (≥15°) and LABs (2-15°), respectively. Thin foils were examined using a Jeol-2010 TEM with a double-tilt stage at an accelerating potential of 200 kV. The TEM was equipped with an X-ray energy-dispersive spectrometer (EDS) produced by Oxford Instruments, Ltd.

Tensile specimens of 25 mm gage length and 3×7 mm^2 cross-section were machined from the aforementioned rods with tension axis lying parallel to the last extrusion direction. These samples were tensioned to failure at room temperature and a strain rate of 2 mm/min using an Instron 5882 testing machine.

3. RESULTS AND DISCUSSION

3.1. Microstructure before ECAP

Typical initial structure of 1570 Al is presented in Fig. 1. The coarse grains with dimensions of ~70 and ~18 μm in longitudinal and transverse directions, respectively, are elongated toward the extrusion axis (Fig.1a). The aspect ratio (AR) of deformed grains is 3.5. The well-defined subgrain structure is observed within these grains (Fig. 1a). Fig. 1b shows the grain size distribution for the initial microstruc-

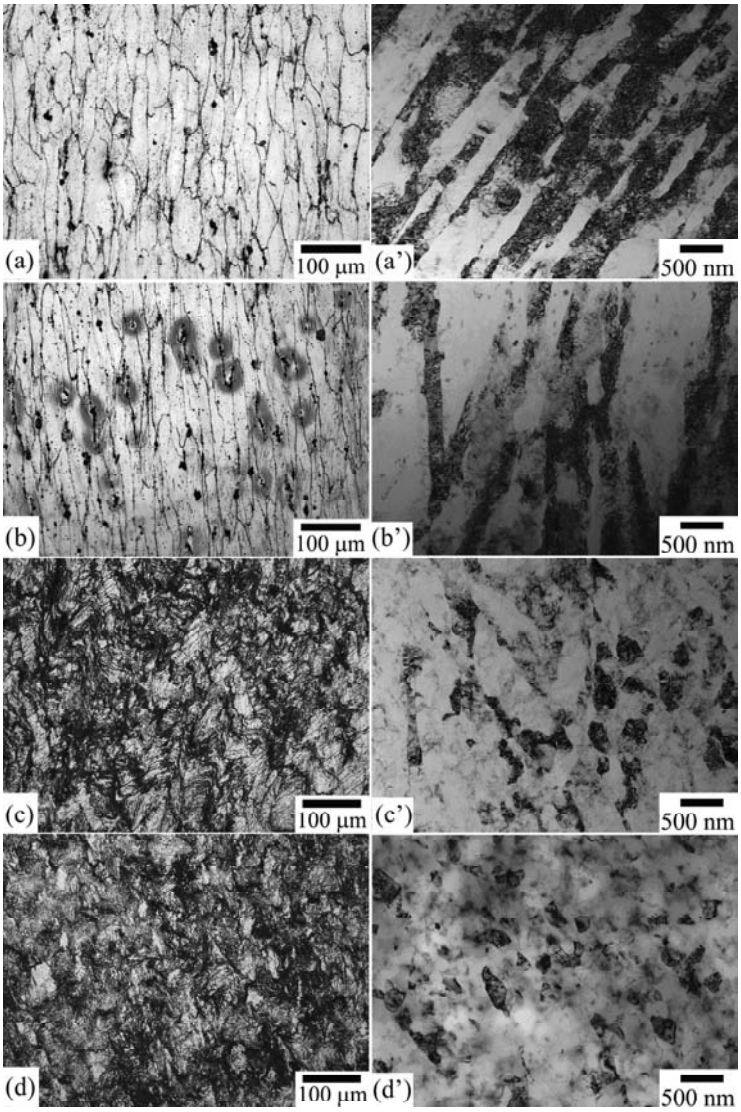

Fig. 2. Typical microstructures of the 1570 alloy after ECAP at 150 °C obtained by the method of (a, b, c, d) optical and (a´, b´, c´, d´) transmission electron microscopy, strained up to (a, a´) ε~1; (b, b´) ~2; (c, c´) ~4, and (d, d´) ~8.

ture, the maximum peak corresponds to the coarse grains with average size ~150 μm and their fraction is higher than 70%. While the fraction of fine grain with size below 2.5 μm is very small and is ~1%. The portion of HAGBs is about 18%; the average misorientation is ~10° (Fig. 1c); and the lattice dislocation density is about $r \sim 1.6 \times 10^{13}$ m^{-2} (Fig. 1d). Two types of second-phase particles were found: coherent dispersoids of $Al_3(Sc,Zr)$ with an average size of~10 nm and incoherent Al_6Mn particles with an average size of~30 nm (Fig. 1d).

3.2. Microstructure evolution during ECAP at 150 °C

Typical microstructures evolved during ECAP are presented in Figs. 2 and 3. After one pass of ECAP the initial grains elongate along the shear direction (Figs. 2a and 3a); their dimensions are of ~60 and ~20 μm in longitudinal and transverse directions, respectively. The deformation substructure is inhomogeneous; two structural components can be distinguished. One component is a bank-like structure of elongated subgrains aligned along the shear direction (Fig. 2a). The other component is made up of fine grains. The formation of microbands with average dimensions of ~10 and ~2 μm in longitudinal and transverse directions, respectively, and outlined partly by LABs and partly by HABs takes place within certain grains (Fig. 3a). In addition, the formation of crystallites with dimensions of ~200 nm in length and ~160 nm in thickness occurs occasionally, however, their volume fraction negligible. It is worth noting that most of deformation-induced

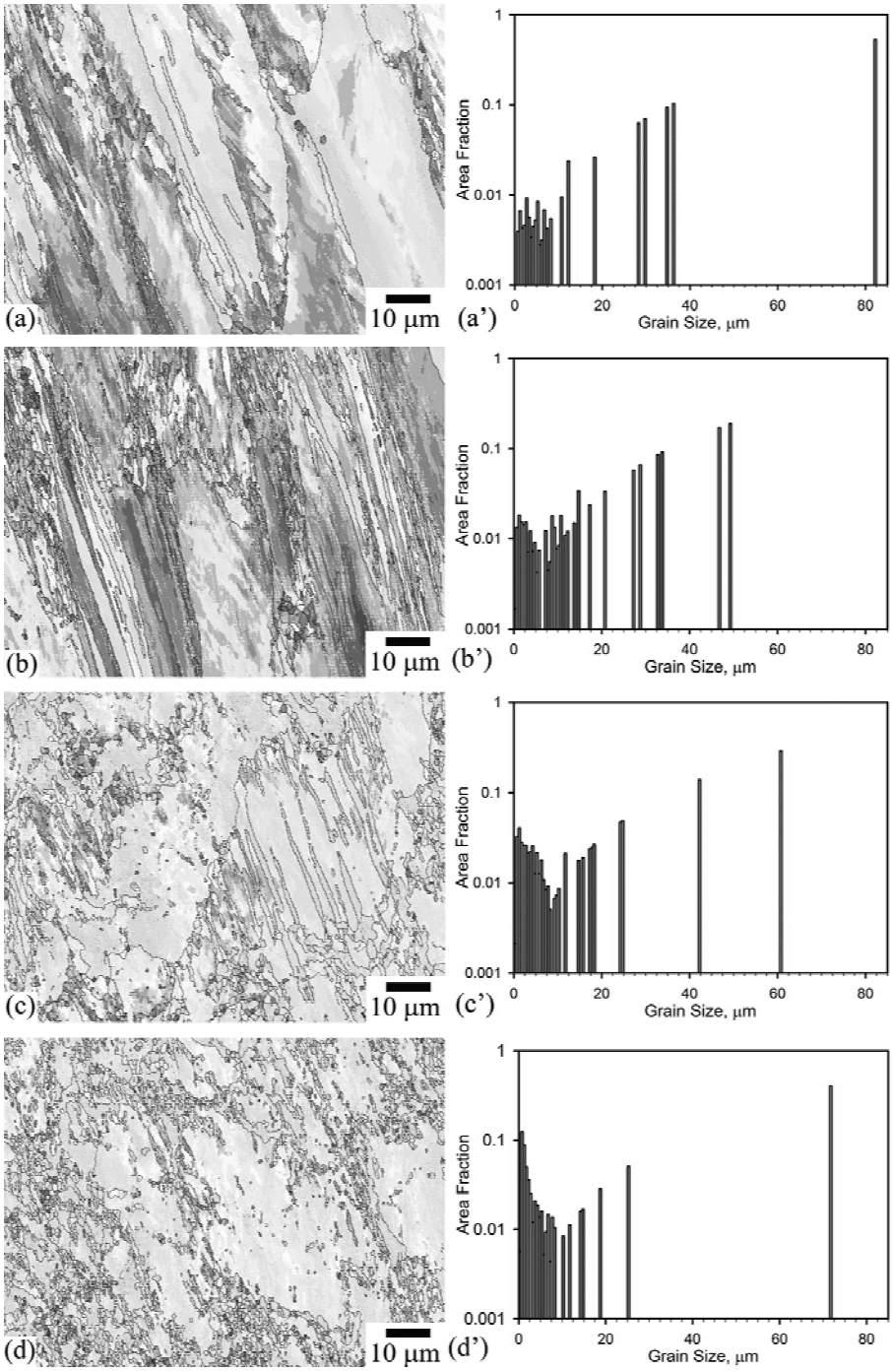

Fig. 3. Typical OIM maps of the microstructure 1570 alloy during ECAP at 150 °C: (a) $\varepsilon \sim 1$, (b) $\varepsilon = 2$, (c) $\varepsilon = 4$, and (d) $\varepsilon = 8$.

boundaries are LABs. Dislocation density within the (sub)grains is $r \sim 2.3 \times 10^{14}$ m^{-2} (Fig. 2a´).

Figs. 3a-3d show the grain size distribution for the deformation microstructures developed at ~1, 2, 4, and 8. It should be noted that the grain size distribution for deformation microstructure in the specimens processed to the all strain are clearly differentiated from the initial one by peaks against small sizes. For example, the sharp peak for grain sizes below 2.5 μm is clearly visible in Fig. 3d. Obviously these peaks are originated from the fine dynamically recrystallized grains. Hereafter, the grains with size of below 2.5 μm are considered as the fine grains. The first pass does not lead to significant change of the size and fraction of new fine grains in comparison with initial state (Fig. 3a). Histograms of measured boundary misorientations are shown in Figs. 4a-4d. The distributions are rather

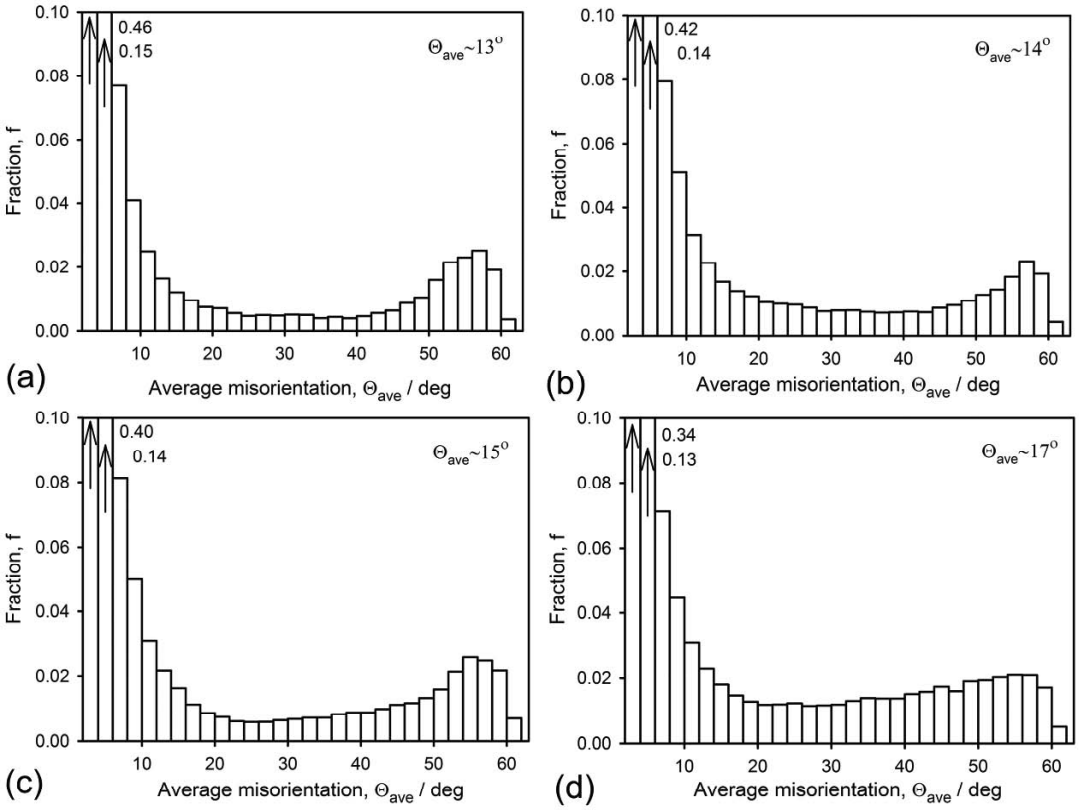

Fig. 4. Misorientation distribution during ECAP for: (a) $\varepsilon \sim 1$, (b) $\varepsilon = 2$ (c), $\varepsilon = 4$, and (d) $\varepsilon = 8$.

flat with 2 peaks, and show only small changes over the strain range. The first peak corresponds to the low angle boundaries with the average misorientation $2 < \Theta < 4°$. The peak height is 0.46 after one ECAP pass; the fraction of high angle boundaries comprising the second peak ranged from 50 to 60° is 53% (Fig. 4a).

After ~2 the average dimensions of course grains decrease to 35 and 21 μm in longitudinal and transverse directions, respectively (Fig. 2b); the evolution of well-defined arrays of deformation-induced boundaries within interiors of almost all initial grains takes place (Fig. 2b´). Average size of submicron scale crystallites remains essentially unchanged, while their volume fraction increases significantly. A number of new fine grains appear along the initial grain boundaries thus making up a mantle surrounding the initial grains (Fig. 3b). The volume fraction of the fine grains with size of below 2.5 μm increases to about 6%; the last maximum corresponds to the coarse grains (average size ~50 μm) taking up ~37% of area fraction (Fig. 3b´). Portion of LABs decreases to 75% (Fig. 4b).

Pressing to a strain of 4 leads to increasing the volume fraction of fine grains. The size of coarse grain decreases to 35 and 19 μm in longitudinal and transverse directions, respectively (Fig. 2c). The average size of the relatively equiaxed (sub)grains is ~140 nm (Fig. 2c´). The (sub)grains are dominating in the microstructure, although the new true fine grains can be also found. The spatial network of LABs is observed within coarse grains (Fig. 3c). The deformation results in the grain refinement (Fig. 3c). The average size of fine grains do not change, while they volume fraction increases to about 13% (Fig. 3c´). The average misorientation is 15°; the portion of HABs is ~27% (Fig. 4c).

Processing to higher strain [~8 leads to the formation of partially recrystallized structure (Fig. 2d-d'). Reminders of original grains with an average size of 17 μm exhibit essentially equiaxed shape. The density of dislocations within the (sub)grains increases to $\rho \sim 4.4 \times 10^{14}$ m^{-2} (Fig. 2d´). In general, HABs are in dominant (Fig. 3d). LABs are observed within relatively coarse grains. The volume fraction of fine grains with size below 2.5 mm increases to about 30% (Fig. 3d´). Relatively low ECAP temperature and the presents of rather large fraction of dispersoids provide stability of the fine grains against coarsening. Fig. 4d shown that the height of the first peak decreases to 0.34 with straining to ~8, while the second peak changes insignificantly. The peak associated with LABs is observed on the misorientation histograms at all strains. LABs con-

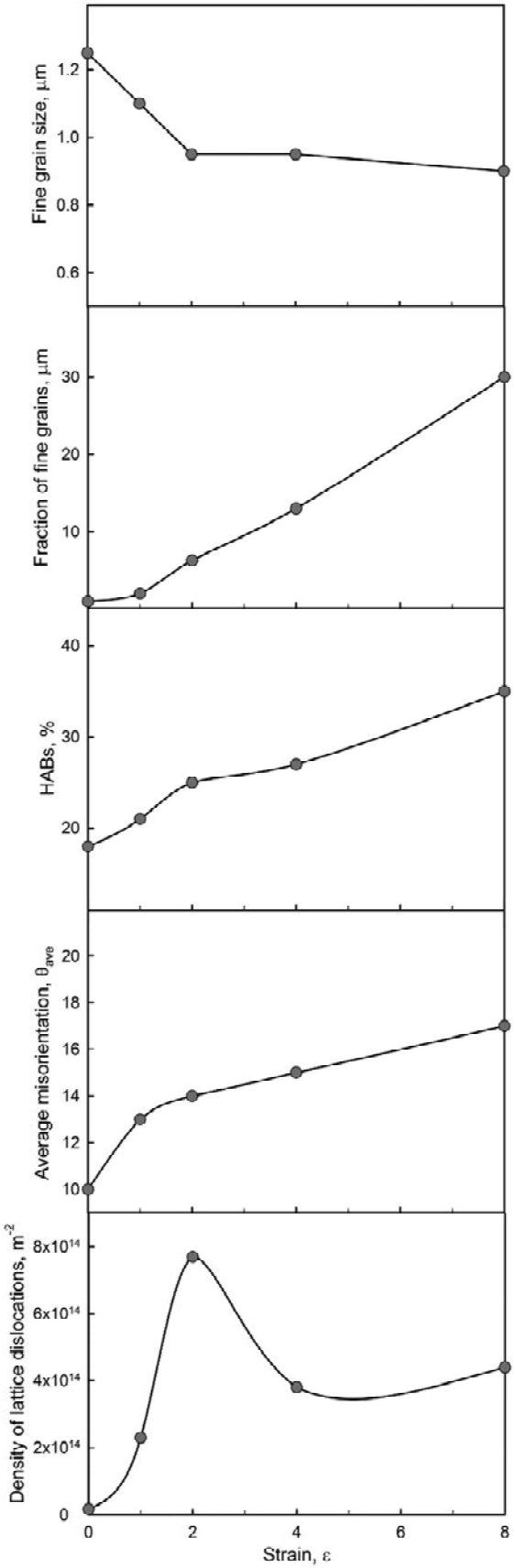

Fig. 5. Effect of strain on the new fine grain size (a); fraction of fine grains (b); population of HABs (c); average misorientation of deformation-induced grain boundaries (d); density of lattice dislocations (e).

tinuously transform into HABs providing a continuous increase in the portion of HABs. As a result, the fraction of HABs increases from 21 to 35% with increasing strain from ~1 to ~8 (Figs. 4a-4d).

3.3. Parameters of the deformed microstructure as a function of strain

The variation of the structural parameters with strain is summarized in Figs. 5a-5e, which shows the effect of strain on the size of new fine grain, the fraction of recrystallized grains, the portion of HABs, the average misorientation and the density of lattice dislocations. These measurements were averaged from several TEM and EBSD maps at each strain level. In the strain interval 1-2 the size of fine grain rapidly decreases to 0.9 μm (Fig. 5). Upon further processing the size of fine grains does not change, however their volume fraction increases with increasing strain. It is seen that at ~1, the formation of recrystallized grains occurs at a low rate due to the fact that the formation of microbands and extended moderate-to-high deformation-induced boundaries (Figs. 3a and 3b) is a processor for the evolution of submicron scale grains. As result, the rate of the formation of these grains is highly accelerated at higher strains (Fig. 5); the fraction of fine grains linear increases from 2 to 30% with increasing strain from ~1 to ~8. It is worth noting that the rate of microstructural evolution during ECAP at 150 °C is significantly less than that at 300 and 450 °C [13].

The data in Fig. 5 clearly demonstrate the moderate rate of grain refinement in the 1570 Al. The HABs portion retains relatively small and comprises about 35% after ~8; and the average misorientation is 17°. However, there exists a distinct feature in evolution of deformation-induced boundaries at 150 °C. In the strain interval 1-8 the average misorientation and the portion of HABs tend to increase with strain and can be expressed by a linear function of cumulated strain. The mean value of dislocation density increases during straining to 2 followed by a somewhat decrease upon further straining to ~4 (Fig. 5). It is apparent that this fact is attributed to transition from planar deformation-induced structure to cellular one (Figs. 2b, 2c, 3b, and 3c). It is worth noting that at $\varepsilon>4$ the lattice dislocation density tends to increase with strain and, therefore, the formation of submicron scale grains does not lead to elimination of lattice dislocation. HABs of these grains exhibit specific extinction counters indicating very high density of grain bound-

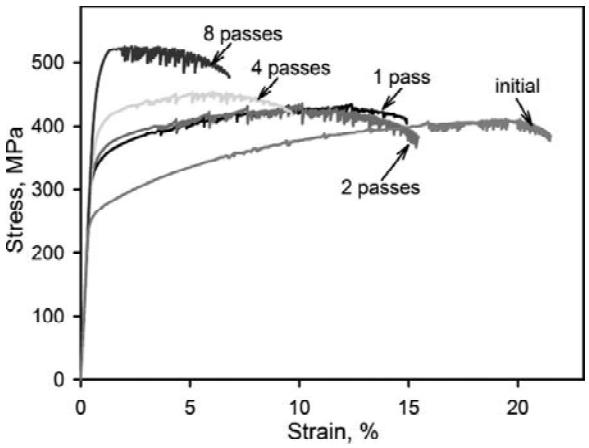

Fig. 6. Mechanical properties of 1570 alloys after ECAP at 150 °C.

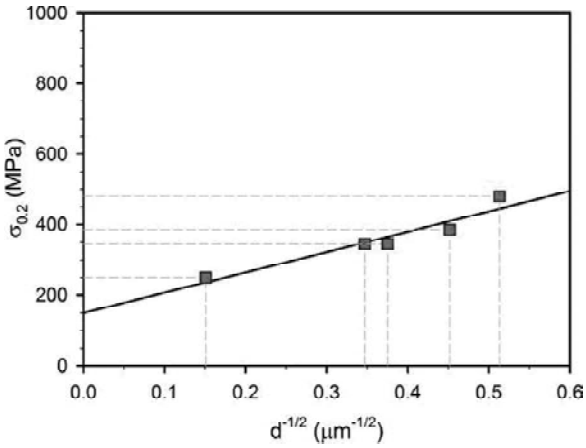

Fig. 7. The Hall-Petch relation for alloy 1570 subjected to ECAP at 150 °C.

ary dislocations [14]. These boundaries are not able to migrate and consume lattice dislocations.

3.4. Mechanical properties after ECAP

Fig. 6 shows the engineering stress-strain curves for the 1570Al; the values of yield stress (YS), ultimate tensile strength (UTS), total elongation and microhardness are summarized in Table 1. All the curves in Fig. 6 exhibit almost similar shape; extensive strain hardening takes place up to failure. The serrated flow is manifested as the repeating oscillations on the stress–strain curves (Fig. 6). This phenomenon is generally associated with the Portevin-Le Chatelier (PLC) effect attributed to dynamic strain aging [16].

After one pass of ECAP the YS increase is +40% in comparison with initial state. Further straining leads to gradual increase in the hardness and the YS. The UTS gradually increases during ECAP up to 8 passes. The ECAP with a total strain of ~8 provides 31, 48, and 23% increases in hardness, YS and UTS, respectively (Table 1). However it is worth noting that threefold decrease in the ductility takes place.

Generally, YS can be related to a grain size through the Hall-Patch relationship [17], which is valid for various recrystallized metals and alloys. The grain size was evaluated by EBSD analysis (with TSL software) to estimate the effect of structural strengthening. Since two structural components are clearly distinguished in the deformation microstructure, i.e. the fine dynamic recrystallized grains and the coarse reminders of original grains, the average mean grain size was calculated as follows:

$$d_{ave} = d_{CG} \times V_{CG} + d_{FG} \times V_{FG}, \quad (2)$$

where d_{CG} and d_{FG} are the size and V_{CG} and V_{FG} are the volume fraction of coarse and fine grains, respectively.

The best fit of experimental results is obtained when σ_0 = 150 MPa and K_y=575 (Fig. 7). Note here that the value of σ_0 = 150 MPa is higher than those of 62 MPa for the alloy Al-3%Mg [10] and 25 MPa for the 1100 alloy [11], but it is close to that of σ_0 = 200 MPa obtained by Valiev [9] for similar alloy.

Table 1. The mechanical properties of the 1570 alloy.

State	YS, MPa	UTS, MPa	δ,%	HV (0.2)
Initial state	250.0	410.0	22.0	110.0
1 pass of ECAP	345.0	430.0	12.0	142.0
2 passes of ECAP	345.0	435.0	15.0	147.0
4 passes of ECAP	385.0	455.0	9.2	151.0
8 passes of ECAP	480.0	530.0	6.4	160.0

4. CONCLUSIONS

Equal-channel angular pressing (ECAP) of the 1570 aluminum alloy at 150 °C results in the grain refinement. The rate of microstructural evolution during ECAP at 150°C is significantly less than at 300-450 °C. The ECAP to a total strain of 8 provides the formation of a partially recrystallized microstructure; the volume fraction of fine grains having a size below 2.5 μm comprises 33%. The deformation substructure is characterized by a relatively large location density of 4.4×10^{14} m^{-2}. The formation of UFG structure and increase dislocation density in the 1570 alloy provides gradual increase in yield stress to 480 MPa.

ACKNOWLEDGEMENTS

This study was supported by Federal Agency for Science and Innovations, Russia, under grant No. 16.740.11.0395. The main results were obtained by using equipment of Joint Research Center, Belgorod State University.

References

[1] R.Z.Valiev and T.G.Langdon // *Prog.Mater.Sci.* **51** (2006) 881.
[2] K.-T. Park, J.H. Park, Y.Sh. Lee and W.J.Nam // *Mater.Sci.Eng*. **A408** (2005) 102.
[3] T.L. Tsai, P.L. Sun, P.W. Kao and C.P. Chang // *Mater.Sci.Eng.* **A342** (2003) 144.
[4] M.A. Munoz-Morris, C. Garsia Oca and D.G. Morris // *Scr.Mater*. **48** (2003) 213.
[5] R. Kapoor and J.K. Chakravartty // *Acta Mater.* **55** (2007) 5408.
[6] J. Gubicza, N.Q. Chinh, T. Csanadi, T.G. Langdon and T.Ungar // *Mater.Sci.Eng.* **A462** (2007) 86.
[7] D.G. Morris and M.A. Munoz-Morris // *Acta Mater.* **50** (2002) 4047.
[8] O.Sh. Sitdikov, E.V. Avtokratova and R.I. Babicheva // *The Physics of Metals and Metallography* **110(2)** (2010) 153.
[9] R.Z. Valiev, N.A. Enikeev, M. Yu. Murashkin, V.U. Kazykhanov and X. Sauvage // *Scripta Materialia* **63** (2010) 949.
[10] M. Furukawa, Z. Horita, M. Nemoto, R.Z. Valiev and T. G. Langdon // *Philos. Mag.* **A 78** (1998) 203.
[11] N. Tsuji, *Nanostructured Materials by High-Pressure Severe Plastic Deformation* (Amsterdam: Springer, 2006), p. 227.
[12] I.A. Mazurina, O.Sh. Sitdikov and R.O. Kaybyshev // *Phys.Metal.Metall*. **94** (2002) 413.
[13] O. Sitdikov, T. Sakai, E. Avtokratova, R. Kaibyshev, Y. Kimura and K. Tsuzaki // *Mater. Sci. Eng.* **444** (2007) 18.
[14] O. Sitdikov, T. Sakai, E. Avtokratova, R.Kaibyshev, K. Tsuzaki and Y. Watanabe // *Acta Mater.* **56** (2008) 821.
[15] R.Kaibyshev, K.Shipilova, F.Musin and Y.Motohashi // *Mater.Sci.Tech.* **21** (2005) 408.
[16] Y. Brechet and Y. Estrin // *Acta Metall. Mater. V*. **43** (1995) 955.
[17] E.O. Hall // *Proc R Soc London, Ser B* **64** (1951) 747.